Nanoscale

Cite this: *Nanoscale*, 2012, **4**, 2078

www.rsc.org/nanoscale

PAPER

Enhancement of biological activities of nanostructured hydrophobic drug species†

Qiusen Han,[a] Rong Yang,*[a] Jingying Li,[a] Wei Liang,[b] Ying Zhang,[a] Mingdong Dong,[c] Flemming Besenbacher[c] and Chen Wang*[a]

Received 16th December 2011, Accepted 19th January 2012
DOI: 10.1039/c2nr12013e

We report a study of nanoribbons of quercetin, a phase I clinical trial anticancer drug, and their inhibitory effects on cancer cell proliferation. Novel quercetin nanoribbons have been prepared by atmospheric pressure physical vapor deposition (PVD). The nanostructures have been characterized by optical microscopy, scanning electron microscopy, transmission electron microscopy, and Raman spectroscopy, *etc.* Significantly enhanced solubility in PBS solution and increased drug release rate have been observed for quercetin nanoribbons in comparison to those of quercetin powder. The observed increase of inhibitory effects of quercetin nanoribbons on 4T1 cancel cell growth is correlated with an improvement in their solubility and drug release behavior.

1. Introduction

Recent progress in nanotechnology has demonstrated its promising potential in disease prevention, diagnosis, imaging, and therapy.[1–3] The use of materials on the nanoscale provides great opportunities to modify some of the fundamental properties of therapeutic ingredients, such as their solubility, diffusivity, distribution and release characteristics.[1,2] In the past decade, a large number of nanoparticle-based therapeutic products, including polymeric nanoparticles, nanocapsules, solid lipid nanoparticles, nanogels and drug nanoparticles have contributed notably to the development of clinical science.[4,5] The nanostructures of these systems allow crossing of biological barriers and improves cellular uptake and transport, thus increasing efficiency of drug delivery to target sites like tumors.[6,7] Moreover, the solubility of nanoscale objects is notably enhanced due to the increased surface-to-volume ratio of nanoparticles.

Quercetin (3,3′,4′,5,7-pentahydroxyflavone) is a phase I clinical trial anticancer drug.[8] It is a unique bioflavonoid that has been extensively studied by researchers over the past 30 years. Bioflavonoids were first discovered by Albert Szent Gyorgyi in 1930.[9] Flavonoids belong to a group of natural substances with variable phenolic structures and are found naturally in fruits, vegetables and beverages such as tea and wine. Quercetin is a well-known flavonoid which belongs to the class of flavonols. It is widely known to have a variety of biological activities and pharmacological actions, such as anti-cancer, anti-oxidation, and anti-inflammation.[10–13] Much *in vitro* research and some preliminary animal and human studies indicate that quercetin inhibits tumor growth.[14–22] For example, quercetin has shown anti-proliferative activities in various tumor cell lines, such as human breast tumor cells,[16,17] human leukemia cancer cells,[19] prostatic carcinoma cells (PC-3),[20] *etc.* The anti-cancer properties of quercetin have been evaluated in a phase I clinical trial in patients.[8] All these studies show that quercetin has an inhibitory effect on tumor growth.

However, quercetin is poorly soluble in water and its bioavailability is very low. Various techniques have been used to increase the solubility of quercetin, such as complexation with cyclodextrin and liposomes.[23,24] However, the use of cyclodextrin is associated with a risk of nephrotoxicity[25] and liposomes are not stable during long-term storage.[26] Therefore, it is clear that more efficient and robust methods of increasing the solubility of quercetin are needed.

The present work is aimed at enhancing the solubility of quercetin through the fabrication of quercetin nanoribbons by atmospheric pressure physical vapor deposition (PVD). Optical microscopy (OM), field emission scanning electron microscopy (FE-SEM), transmission electron microscopy (TEM), and Raman spectroscopy were used to characterize the structure of the nanoribbons. Solubility in PBS solution and the total amount released from quercetin nanoribbons were compared to those of quercetin powder. Cell viability studies were conducted on 4T1 mouse breast cancer cells. The relationship between the enhanced inhibition effect on cancer cells and the properties of quercetin nanoribbons will be discussed.

[a]*CAS Key Lab for Biomedical Effects of Nanomaterials and Nanosafety, National Center for Nanoscience and Technology, Beijing, 100190, China. E-mail: yangr@nanoctr.cn; wangch@nanoctr.cn*
[b]*Institute of Biophysics, Chinese Academy of Sciences, Beijing, 100101, China*
[c]*Interdisciplinary Nanoscience Center, Aarhus University, Denmark*
† Electronic supplementary information (ESI) available. See DOI: 10.1039/c2nr12013e

2. Experimental details

2.1. Fabrication of quercetin nanoribbons

Quercetin nanoribbons were fabricated by atmospheric pressure PVD. The quercetin powder (99.99% pure) used in this work was purchased from Alfa Co. The fabrication of quercetin nanoribbons was carried out in a conventional tube furnace at about 280 °C, with an argon flow-rate of about 80 sccm. Quercetin powder was loaded into a quartz boat and placed in the middle of a quartz tube. Silicon substrates were arranged downstream of the quartz tube to collect the products. The growth process lasted for 60 min, and then the furnace was cooled to room temperature under argon gas.

2.2. Characterization

The quercetin nanoribbons were characterized by optical microscopy (Leica, DM4000), field emission scanning electron microscopy (FE-SEM; Hitachi S-4800), transmission electron microscopy (TEM; Tecnai G220 ST), UV-Vis spectrometry (Lambda950; UV/VIS/NIR), Raman spectroscopy (Renishaw, the excitation wavelength was 632.8 nm), *etc.*

2.3. Solubility measurement

The solubilities of quercetin nanoribbons and quercetin powder in PBS solution were measured at room temperature. Firstly, standard solutions of quercetin were prepared by adding quercetin powder into dimethyl sulfoxide (DMSO) at different concentrations (0.2, 0.4, 0.8, 1, 2, 4, 6, and 8 μg ml^{-1}) in a volume of 2.0 ml. Secondly, the absorbance of each solution was measured using a UV-Vis spectrometer with a wavelength of 367 nm. Thirdly, a calibration curve was drawn according to the data of quercetin absorbance and concentration.

A saturated solution of quercetin nanoribbons in PBS was prepared to evaluate its solubility. The solution was shaken with rotation speed of 218 rpm at room temperature for 48 h. After that, it was filtered with a 0.45 μm filter and then centrifuged. A portion of the supernatant (5 ml) was selected and the liquid was removed by slow evaporation, followed by adding 5 ml DMSO, which represents the concentration of the saturated solution. The absorbance of the solution in DMSO was then measured with a UV-Vis spectrometer. The concentration of the saturated PBS solution of quercetin nanoribbons was then calculated from the measured absorbance, the linear regression equation of the calibration curve, and the dilution factor. The solubility of quercetin powder in PBS solution was measured in a similar way.

2.4. Cell culture

4T1 cell lines were mouse breast cancer cells, which were seeded on three different surfaces (Si, quercetin powder/Si and quercetin ribbons/Si). Before use, each substrate was sterilized with UV for 30 min and cleaned in 70% ethanol and deionized water. 4T1 cells were cultured in DMEM medium (Hyclone) with 10% (v/v) heat-inactivated fetal calf serum (FCS, Sigma), 100 IU ml^{-1} penicillin, and 100 μg ml^{-1} streptomycin. The culture plates were incubated at 37 °C in a humidified incubator containing 5% CO_2.

2.5. Cell viability assay by fluorescence microscopy

4T1 cells (2×10^4 cells ml^{-1}) were cultured in 24-well plates and on different surfaces as discussed above. After 24 h, the cells were labeled by incubation with acridine orange (Sigma Aldrich) at a concentration of 100 μg ml^{-1} for 20 min at 37 °C in the dark. After incubation, the cells were washed with cold PBS solution three times and examined under a fluorescence microscope (Leica, Germany). For each sample, three sections were selected and examined randomly. Excitation was performed by an argon ion laser operating at 488 nm and the emitted fluorescence was collected through a 515 nm pass filter.

3. Results and discussion

Fig. 1 shows optical micrographs of quercetin nanoribbons on Si substrate prepared by atmospheric pressure PVD. The Si substrate is uniformly covered by quercetin nanoribbons. The nanoribbons are uniform in size, and no aggregation is observed. The technique of PVD is a feasible and effective method to prepare nanoribbons of quercetin. This technique could be scaled up when the experimental conditions are changed, for example, using low pressure PVD.

The molecular structure of quercetin is shown in the inset of Fig. 1. Quercetin consists of two aromatic rings (A and B) linked by an oxygen containing heterocycle (ring C), and it possesses 5 hydroxyl groups.

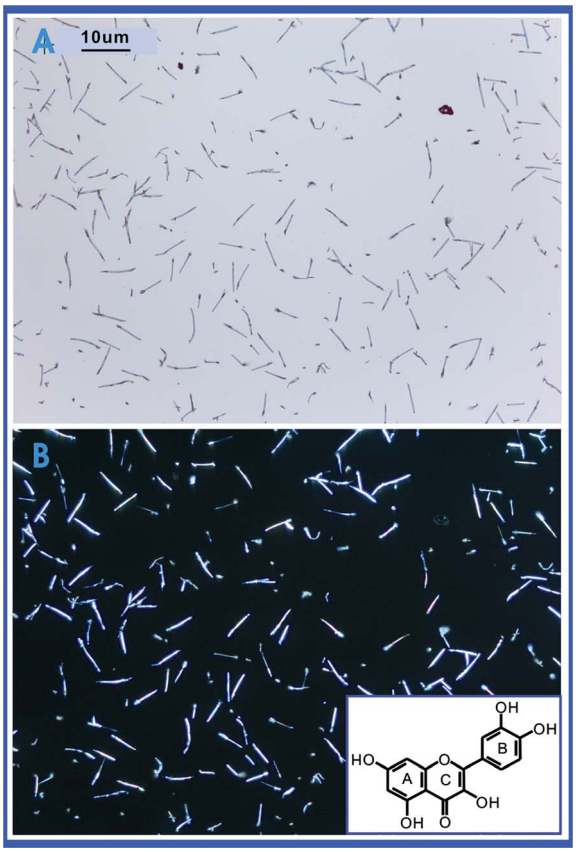

Fig. 1 The optical micrographs of quercetin nanoribbons. (A) is a bright field optical micrograph; (B) is a dark field optical micrograph. The molecular structure of quercetin is shown in the inset.

The morphology of quercetin nanoribbons was further characterized by SEM and TEM. The average width of the quercetin nanoribbons is around 100–200 nm. The inset in Fig. 2A is a TEM image of a single quercetin nanoribbon. Fig. 2B displays the UV-Vis absorption spectrum of quercetin nanoribbons in water. In the range of 200–450 nm, two characteristic absorption bands can be seen: a band around 367 nm (Band I) representing the B-ring absorption, and another one around 254 nm (Band II) representing the A-ring absorption.[27,28] The UV-Vis absorption spectrum of quercetin powder in DMSO is also shown in Fig. 2B.

Raman spectra of quercetin nanoribbons and quercetin powder are shown in Fig. 3. The samples show typical Raman scattering bands of quercetin, which correspond well to those described in the literature.[29–35] In general, the spectrum below 1000 cm^{-1} is due to the skeletal structure. The region at 1660–1550 cm^{-1} is attributed to the ν(C═O) and ν(C═C) vibrations. Bands in the 1400–1000 cm^{-1} region are due to the δ(O–H) and ν(C–O) vibrations of different OH groups.

The solubilities of quercetin nanoribbons and quercetin powder in PBS solution were measured at room temperature.

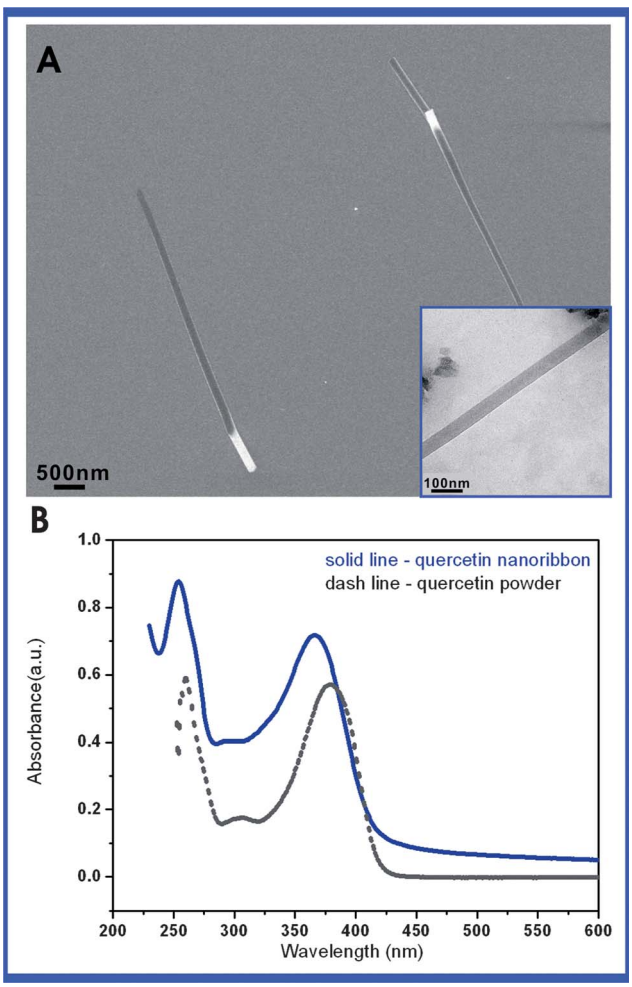

Fig. 2 The SEM, TEM image and UV-Vis absorption spectra of quercetin nanoribbons and powder. (A) The SEM image of quercetin nanoribbons, a TEM image of a single quercetin ribbon is shown in the inset; (B) UV-Vis absorption spectra of quercetin nanoribbons (solid line) and quercetin powder (dashed line).

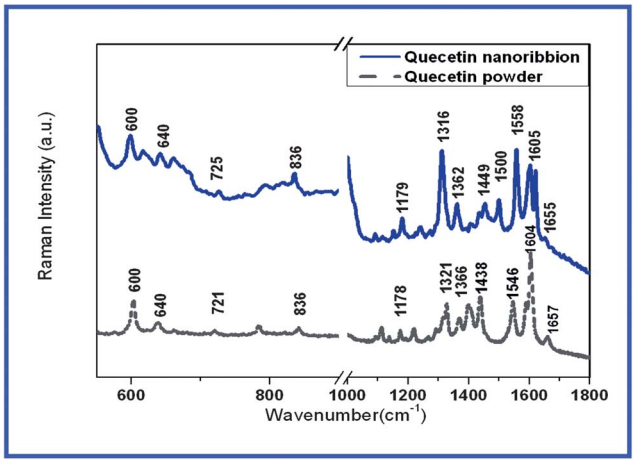

Fig. 3 Raman spectra of quercetin nanoribbons (solid line) and quercetin powder (dashed line).

Fig. 4 shows a comparison of PBS solubility between quercetin nanoribbons and powder. One can see that the PBS solubility of quercetin nanoribbons was significantly increased compared with that of quercetin powder. The increased surface-to-volume ratio of the nanoribbons may have contributed to the observed improvement in the solubility of the drug. A comparison of the SEM images and optical micrographs of quercetin nanoribbons and powder are shown in Fig. S1 and Fig. S2 in the ESI.†

Fig. 5 shows release profiles of the quercetin nanoribbons and quercetin powder in PBS. For quercetin powder, less than 1% of the total drug was released in the first hour. The release profile reached saturation at about 2 h with 1.3% released. In contrast, for quercetin nanoribbons, 3% of the total drug was released in the first hour and a total of 13% was released in the following 7 h before reaching saturation. As can be seen in the release profile, in comparison to quercetin powder, ten times more quercetin was released from the nanoribbons. Furthermore, quercetin nanoribbons maintained a continuous release over 8 h, making them attractive for controlled release of quercetin. The characteristic

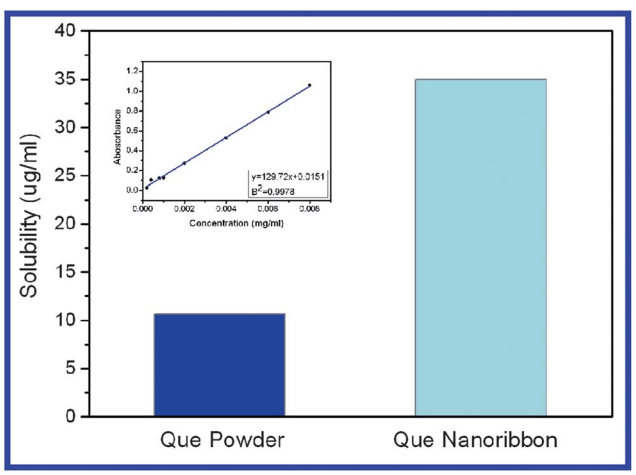

Fig. 4 Comparison of PBS solubility between quercetin powder and quercetin nanoribbons. The calibration curve is shown in the inset of Fig. 4.

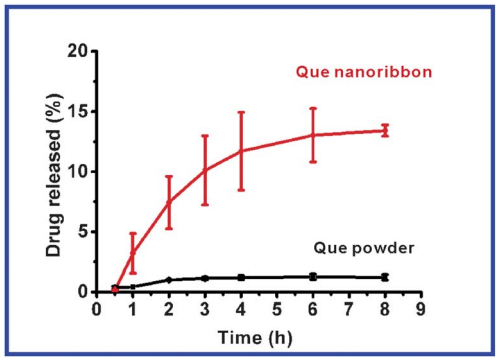

Fig. 5 Comparison of drug release profiles between quercetin powder and quercetin nanoribbons.

releasing behavior of quercetin nanoribbons is probably due to the significantly reduced size and consequently greatly increased surface-to-volume ratio of the drug.

To study the effect of quercetin nanoribbons on cancel cell growth, 4T1 cells were labeled (mouse breast cancer cell) with acridine orange (Sigma Aldrich) and cell viability and proliferation were studied under a fluorescence microscope. 4T1 cells were cultured in 24-well plates and incubated on three different surfaces (Si, quercetin powder/Si and quercetin nanoribbons/Si) for 48 h. Fig. 6 shows the fluorescence microscopy images of 4T1 cells on these three surfaces. On the Si substrate (Fig. 6A), the cells grew very well, indicating that the Si substrate was biocompatible and non-toxic to cell proliferation. On the quercetin powder/Si surface, less cells were observed, indicating that quercetin powder had inhibitory effort on 4T1 cells. On the quercetin nanoribbons/Si surface, however, cell numbers were significantly lower. As shown in Fig. 7, the quercetin powder and quercetin nanoribbon covered surfaces reduced the cell number by 32% and 57%, respectively. In conclusion, quercetin nanoribbons inhibited cancer cell growth more efficiently than quercetin powder.

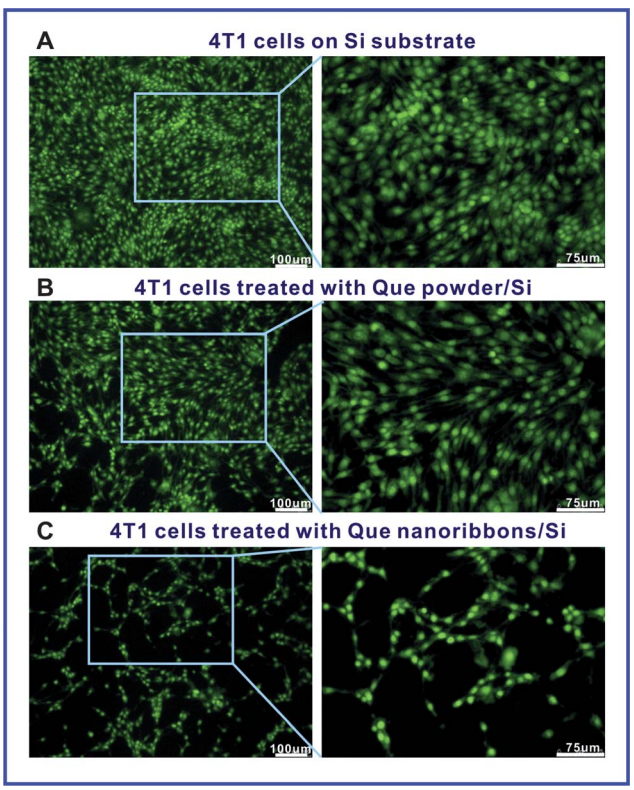

Fig. 6 The fluorescence microscopy images of 4T1 cells cultured for 48 h on different surfaces. (A) 4T1 cells on Si substrate (control surface); (B) 4T1 cells on quercetin powder/Si surface; (C) 4T1 cells on quercetin nanoribbons/Si surface. The right-side column images are magnification images of box regions of left-side column images.

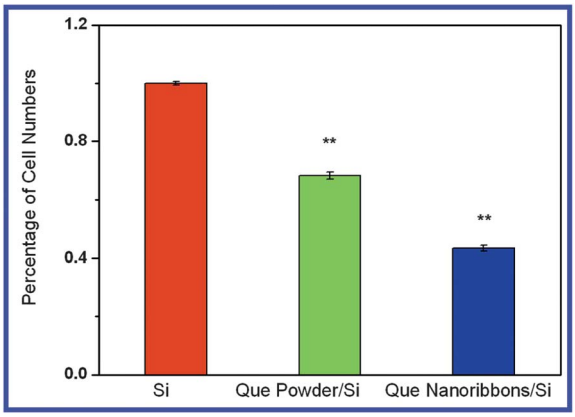

Fig. 7 The percentage of 4T1 cell numbers on different surfaces. The sample sizes were 1 cm × 1 cm (The cell numbers were counted from the fluorescence microscopy images shown in Fig. 6.). ** indicates statistical significance ($P < 0.01$) when compared to the control.

4. Conclusion

In summary, quercetin nanoribbons have been successfully fabricated by atmospheric pressure PVD. Structural analysis revealed well defined, uniform nanoribbon structures. Both the solubility in PBS and the drug release amount and time were significantly enhanced, which was attributed to the reduction of drug size and, therefore, an increase in the surface-to-volume ratio of the drug. Cell viability studies showed that the quercetin nanoribbons inhibited 4T1 cancer cell growth significantly compared to quercetin powder. The technique of PVD provides a straightforward, feasible and effective method to produce nanosized drugs with improved solubility, drug release behavior and anti-cancer ability.

Acknowledgements

This work was supported by the National Natural Science Foundation of China (20911130229, 21073047) and the Chinese Academy of Sciences (KJCX2.YW.M15).

References

1 D. F. Emerich and C. G. Thanos, *J. Drug Targeting*, 2007, **15**, 163–83.
2 (*a*) D. A. Groneberg, M. Giersig, T. Welte and U. Pison, *Curr. Drug Targets*, 2006, **7**, 643–648; (*b*) V. Wagner, A. Dullaart, A.-K. Bock and A. Zweck, *Nat. Biotechnol.*, 2006, **24**, 1211–1217.
3 S. M. Sagnella, X. Gong, M. J. Moghaddam, C. E. Conn, K. Kimpton, L. J. Waddington, I. Krodkiewska and C. J. Drummond, *Nanoscale*, 2011, **3**, 919–924.

4 L. Zhang, F. X. Gu, J. M. Chan, A. Z. Wang, R. S. Langer and O. C. Farokhzad, *Clin. Pharmacol. Ther.*, 2008, **83**, 761–769.
5 L. Zhang, J. M. Chan, F. X. Gu, J. Rhee, A. Z. Wang, A. F. Radovic-Moreno, F. Alexis, R. Langer and O. C. Farokhzad, *ACS Nano*, 2008, **2**, 1696–1702.
6 (*a*) T. Nakamura, A. Tamura, H. Murotani, M. Oishi, Y. Jinji, K. Matsuishi and Y. Nagasaki, *Nanoscale*, 2010, **2**, 739–746; (*b*) W. E. Bawarski, E. Chidlowsky, D. J. Bharali and S. A. Mousa, *Nanomed.: Nanotechnol., Biol. Med.*, 2008, **4**, 273–282.
7 S. M. Moghimi, A. C. Hunter and J. C. Murray, *Pharmacol. Rev.*, 2001, **53**, 283–318.
8 D. W. Lamson and M. S. Brignall, *Altern. Med. Rev.*, 2000, **5**, 196–206.
9 P. Lakhanpal and D. K. Rai, *Internet J. of Medical Update*, 2007, **2**, 22–37.
10 N. Gulati, B. Laudet, V. M. Zohrabian, R. Murali and M. Jhanwar-Uniyal, *Anticancer Res.*, 2006, **26**, 1177–1181.
11 D. W. Lamson and M. S. Brignall, *Altern. Med. Rev.*, 2000, **5**, 196–206.
12 A. Schlachterman, F. Valle, K. M. Wall, N. G. Azios, L. Castillo, L. Morell, A. V. Washington, L. A. Cubano and S. F. Dharmawardhane, *Translational Oncology.*, 2008, **1**, 19–27.
13 P. C. Hollman and M. B. Kata, *Food Chem. Toxicol.*, 1999, **37**, 937–942.
14 A. M. S. Silva, P. Filipe, R. S. G. R. Seixas, D. C. G. A. Pinto, L. K. Patterson, G. L. Hug, J. A. S. Cavaleiro, J. Maziere, R. Santus and P. Morliere, *J. Phys. Chem. B*, 2008, **112**, 11456–11461.
15 G. Zhang, B. Keita, J. Brochon, P. Oliveira, L. Nadjo, C. T. Craescu and S. Miron, *J. Phys. Chem. B*, 2007, **111**, 1809–1814.
16 S. Khoee, S. Hassanzadeh and B. Goliaie, *Nanotechnology*, 2007, **18**, 175602–11.
17 S. M. Plakas, T. C. Lee and R. E. Wolke, *Food Chem Toxicol*, 1985, **2**, 1077–80.
18 R. L. Singhal, Y. A. Yeh and N. Prajda, *et al.*, *Biochem. Biophys. Res. Commun.*, 1995, **208**, 425–431.
19 F. V. So, N. Guthrie and A. F. Chambers, *et al.*, *Nutr. Cancer*, 1996, **26**, 167–181.
20 G. Agullo, L. Gamet and C. Besson, *et al.*, *Cancer Lett.*, 1994, **87**, 55–63.
21 G. Scambia, F. O. Ranelletti and P. P. Benedetti, *et al.*, *Br. J. Cancer*, 1990, **62**, 942–946.
22 M. Russo, C. Spagnuolo, S. Volpe, A. Mupo, I. Tedesco and G.-L. Russo, *Br. J. Cancer*, 2010, **103**, 642–648.
23 M. R. Vijayababu, P. Kanagaraj, A. Arunkumar, R. Ilangovan, M. M. Aruldhas and J. J. Arunakaran, *J. Cancer Res. Clin. Oncol.*, 2005, **131**, 765–771.
24 N. Gulati, B. Laudet, V. M. Zohrabian, R. Murali and M. Jhanwar-Uniyal, *Anticancer Res.*, 2006, **26**, 1177–1181.
25 A. Schlachterman, F. Valle, K. M. Wall, N. G. Azios, L. Castillo, L. Morell, A. V. Washington, L. A. Cubano and S. F. Dharmawardhane, *Translational Oncology*, 2008, **1**, 19–27.
26 L. Chebil, C. Chipot, F. Archambault, C. Humeau, J. M. Engasser, M. Ghoul and F. Dehez, *J. Phys. Chem. B*, 2010, **114**, 12308–12313.
27 T. Pralhad and K. Rajendrakumar, *J. Pharm. Biomed. Anal.*, 2004, **34**, 333–339.
28 Z. P. Yuan, L. J. Chen, L. Y. Fan, M. H. Tang, G. L. Yang, H. S. Yang, X. B. Du, G. Q. Wang, W. X. Yao and Q. M. Zhao, *et al.*, *Clin. Cancer Res.*, 2006, **12**, 3193–3199.
29 H. W. Frijlink, A. C. Eissens, N. R. Hefting, K. Poelstra, C. F. Lerk and D. K. Meijer, *Pharm. Res.*, 1991, **8**, 9–16.
30 X. Mu and Z. Zhong, *Int. J. Pharm.*, 2006, **318**, 55–61.
31 A. Torreggiani, M. Tamba, A. Trinchero and S. Bonora, *J. Mol. Struct.*, 2005, **744**, 759–766.
32 Z. Ferenc, B. Zsolt and S. Miklos, *Biochem. Pharmacol.*, 2003, **65**, 447–456.
33 Z. Jurasekova, J. V. Garcia-Ramos, C. Domingo and S. Sanchez-Cortes, *J. Raman Spectrosc.*, 2006, **37**, 1239–1241.
34 T. Teslova, C. Corredor, R. Livingstone, T. Spataru, R. L. Birke, J. R. Lombardi, M. V. Canamares and Marco. Leona, *J. Raman Spectrosc.*, 2007, **38**, 802–818.
35 J. P. Cornard and J. C. Merlin, *J. Inorg. Biochem.*, 2002, **92**, 19–27.

